Formulating Reduced Density Gradient Approaches for Noncovalent Interactions

Cristian Guerra,[*,†] José Burgos,[*,†] Leandro Ayarde-Henríquez,[*,‡,¶] and Eduardo Chamorro[*,†,§]

†*Universidad Andrés Bello. Facultad de Ciencias Exactas. Departamento de Ciencias Químicas. Avenida República 275, 8370146, Santiago de Chile, Chile.*

‡*School of Physics, Trinity College Dublin, Dublin 2, Ireland.*

¶*AMBER, Advanced Materials and BioEngineering Research Centre, Dublin 2, Ireland.*

§*Universidad Andrés Bello. Centro de Química Teórica y Computacional (CQTC). Facultad de Ciencias Exactas. Departamento de Ciencias Químicas. Avenida República 275, 8370146, Santiago de Chile. Chile*

E-mail: c.guerramadera@uandresbello.edu; j.burgosmoreno@uandresbello.edu; leandro.ayarde@tcd.ie; echamorro@unab.cl

Keywords:Non-covalent interactions; local moments; kinetic energy density; reduced density gradient.

Abstract

This work elucidates several forms of reduced electron density gradient (RDG) to describe non-covalent interactions (NCIs). By interpreting the RDG as a local-moment function, we systematically leveraged Weizacker's and Fermi's local moments. This resulted in high-fidelity RDG representations consistent with the NCI analysis. In addition, the RDG version derived from the Lagrangian kinetic energy density is conveniently normalized. These results suggest the non-existence of a particular RDG

formulation when performing NCI analysis. Thus, an in-depth examination of the theoretical foundations connecting the RDG function with the nature of non-covalent interactions is necessary.

Introduction

Real-space functions have successfully connected empirical evidence with physical and chemical phenomena.[1,2] In particular, electron density-based functions such as the electronic localization function (ELF)[3,4] and the reduced gradient of the electron density (RDG)[5] exemplify some of the most widely utilized physicochemical models for scrutinizing electronic structure properties, including chemical bonding,[6,7] reactivity,[8,9] and interaction energies.[10] ELF's bonding analysis has extensively provided fundamental mechanistic insights into electron rearrangements,[11–13] cycloadditions,[14–19] photoreactions,[20–26] distinct covalent bonding scenarios,[27,28] and pyrolytic processes.[29–31] Additionally, this framework has proven instrumental in developing models to predict activation barriers of both organic and organometallic systems.[32] Conversely, several indices have been proposed for studying atomic interactions in the DFT context, covering the weak-to-strong spectrum. The non-covalent interaction (NCI)[5] index was elucidated to characterize the weak portion, the bonding and non-covalent index (BNI)[33,34] was designed to describe the weak-to-moderate range, the strong covalent interaction (SCI)[35] index was proposed to gain information on the moderate-to-strong interval, and the ultra-strong interaction (USI)[33] index was derived to identify strong interactions. In particular, NCI analysis based on RDG has been diverse and impactful across various fields such as chemistry, biology, and material science, including systems in both the gas phase and solid state. Its main advantage lies in the fast characterization of non-covalent interactions based on the curvature of the electron density. Even the promolecular approach is compatible with RDG, allowing the study of large molecular systems. In this context, NCI has emerged as a popular tool for assessing properties of crystals,[36–38] in drugs[39,40] and materials discovery,[41,42] testing electrochemical sensors,[43] in biological studies,[44,45] investi-

gating racemization[46] and organocatalytic mechanisms,[47] as well as exploring hydrogen[48] and halogen bonds.[49]

A prevalent issue in developing new scalar fields is *the clarity of their physical foundations and formal derivation*. The well-known reduced electron density gradient $s(\mathbf{r})$[50–53] exemplifies this situation:

$$s(\mathbf{r}) = \frac{1}{2(3\pi^2)^{1/3}} \frac{\nabla\rho(\mathbf{r})}{\rho(\mathbf{r})^{4/3}} \tag{1}$$

Notably, the nature of these interactions is characterized by the electron density curvature over regions defined by $s(\mathbf{r})$. This dimensionless quantity was initially derived from the generalized gradient approximation (GGA)[54,55] to fine-tune the performance of functionals:

$$E[\rho]_X^{GGA} = \int d\mathbf{r} \epsilon_X^{LDA}(\mathbf{r}) F_X^{GGA(s)} \tag{2}$$

Both ϵ_X^{LDA} and $F_X^{GGA}(s)$ have a clear physical interpretation within the framework of density functional theory (DFT).[56,57] However, no relationship between NCI and RDG can be anticipated. Indeed, the nonexistence of a formal demonstration connecting RDG with the physicochemistry of NCI has led to misinterpretations[58] and algebraic modifications of RDG[59] lacking physical rigor. On the other hand, $s(\mathbf{r})$ contributes to estimating energy rather than describing the physics of NCIs directly. For DFT applications, $s(\mathbf{r})$ is crucial as it effectively incorporates the inhomogeneity of the electron density into the exchange-correlation functionals.[60] Extracting $s(\mathbf{r})$ from the energy density functional $E[\rho]_X^{GGA}$ and its further use as an NCI descriptor raises challenging questions: (i) Does $s(\mathbf{r})$ represent a property of a quantum system? No. Despite its dependence on the observable ρ, $s(\mathbf{r})$ does not inherently represent fundamental physical quantities like momentum or energy as it is unlinked to a quantum observable. (ii) Is the RDG based on realistic physicochemical models? To some extent. The RDG can be written as an algebraic relationship between kinetic energy densities (KED).[61–65] as follows:

$$\frac{\tau_W(\mathbf{r})}{\tau_{TF}(\mathbf{r})} = \frac{5}{3}s(\mathbf{r})^2 \tag{3}$$

Contreras and coworkers[52,53] found this relation between $s(\mathbf{r})$ and the Von Weizsacker (WZ)[66–69] $\tau_W(\mathbf{r})$ and Thomas-Fermi (TF)[70–72] $\tau_{TF}(\mathbf{r})$ KEDs. The first KED describes a bosonic system, while the other represents a gas of non-interacting electrons. The nexus between $s(\mathbf{r})$ and KEDs is evidenced by equation (3). It is worth mentioning that $\tau_W(\mathbf{r})$ and $\tau_{TF}(\mathbf{r})$ are derived from physical models under ideal considerations. The WZ model was initially conceived to correct the significant overestimation in the kinetic energy density of molecular systems given by the TF model.[56] One might assume that, due to the direct dependence of $s(\mathbf{r})$ on $\rho(\mathbf{r})$, it would suffice to solve any N-electron problem and obtain a high-quality density in order to calculate $s(\mathbf{r})$ regardless of the level of theory (e.g., DFT, MP2, CASSCF, CCSD, and MRCI). Nevertheless, issues inherent to the descriptions provided by either $\tau_W(\mathbf{r})$ or $\tau_{TF}(\mathbf{r})$ are encapsulated within $s(\mathbf{r})$.

(iii) Considering the arbitrary use of RDG to describe non-covalent interactions, is there space for conceptual improvements? Yes. More accurate energies are obtained using DFT by a linear combination of WZ and TF, $\alpha\tau_{TF}(\mathbf{r})+\beta\tau_{WZ}(\mathbf{r})$.[54–56,64,68] This entails the feasible derivation of new forms of $s(\mathbf{r})$, which poses concerns about its uniqueness and optimal expression for describing NCIs. These challenges will remain open to further investigations that must focus on establishing $s(\mathbf{r})$ as a quantum property. This manuscript discusses the conceptual limitations of the original RDG and proposes alternative ways of designing this function to perform NCI analysis, stressing that the RDG should not be restricted to one type of computation. By exploring the direct relationship between $\tau(\mathbf{r})$ and $s(\mathbf{r})$, we improve the description provided by $s(\mathbf{r})$ by refining the $\tau(\mathbf{r})$, with particular emphasis on $\tau_{TF}(\mathbf{r})$ and $\tau_{WZ}(\mathbf{r})$. Furthermore, the suitability of various representations of $\tau^n_{TF}(\mathbf{r})$ and τ^n_{WZ} to construct $s(\mathbf{r})$ is assessed. The performance of the derived RDG in characterizing non-covalent interactions is also evaluated.

Methodology

We have carefully considered several corrections to $\tau_{TF}(\mathbf{r})$ and $\tau_{WZ}(\mathbf{r})$[67,69] to derive the new forms of $s(\mathbf{r})$, as KEDs are the most challenging component to model in the DFT domain:

$$\tau^1_{WZ}(\mathbf{r}) = \frac{1}{9}\tau_{WZ}(\mathbf{r}) \tag{4}$$

$$\tau^1_{TF}(\mathbf{r}) = \left(1 - \frac{C}{N^{1/3}}\right)\tau_{TF}(\mathbf{r}) \tag{5}$$

$$\tau^2_{TF}(\mathbf{r}) = \left(1 - \frac{2}{N}\right)\left(1 - \frac{C_0}{N^{1/3}} - \frac{C_1}{N^{2/3}}\right)\tau_{TF}(\mathbf{r}) \tag{6}$$

In equation (4), τ^1_{WZ} is the Weizacker kinetic energy density derived from the power series expansion of the kinetic energy functional, which has demonstrated good performance within the framework of GGA.[55,73] Conversely, τ^1_{TF} and τ^2_{TF} represent the adjustments made to the Thomas-Fermi kinetic energy density by Acharya and Gazquez, respectively.[67,69] C, C_0, and C_1 represent numerical constants with values 1.412, 1.015, and 0.150, respectively. It is widely recognized that $\tau(\mathbf{r})$ is typically used to describe chemical bonding rather than non-covalent interactions. Thus, we have opted to define $s(\mathbf{r})$ using Cohen's notation[74] for local moments, contrary to KED notation:

$$s^1(\mathbf{r}) = \frac{|P_{WZ}(\mathbf{r})|}{P_{TF}(\mathbf{r})} \tag{7}$$

where $P_{WZ}(\mathbf{r})$ is the local monoelectronic momentum,[75,76] hereafter referred to as Weizacker's momentum. Additionally, $P_{TF}(\mathbf{r})$ represents Thomas-Fermi's momentum. This paper considers also the following expressions for $s(\mathbf{r})$:

$$s^2(\mathbf{r}) = \frac{1}{6}\frac{P_{WZ}(\mathbf{r})}{P_{TF}(\mathbf{r})} \tag{8}$$

$$s^3(\mathbf{r}) = \frac{1}{6}\frac{P_{WZ}(\mathbf{r})}{\sqrt{\left(1-\frac{C}{N^{1/3}}\right)}P_{TF}(\mathbf{r})} \tag{9}$$

$$s^4(\mathbf{r}) = \frac{1}{6}\frac{P_{WZ}(\mathbf{r})}{\sqrt{\left(1-\frac{2}{N}\right)\left(1-\frac{C_0}{N^{1/3}}+\frac{C_1}{N^{2/3}}\right)}P_{TF}(\mathbf{r})} \tag{10}$$

These equations resulted from approximations for $\tau_{TF}(\mathbf{r})$ and $\tau_{WZ}(\mathbf{r})$, and can be found in the available literature.[55,56,64,68] Detailed information regarding the derivation of $s^n(\mathbf{r})$ is available in the Electronic Supplementary Information (ESI). It is crucial to emphasize that these models are conceptually more robust than both the Thomas-Fermi and Weizacker derivations. The 1/6 term added to $P_{WZ}(\mathbf{r})$ comes from the gradient expansion performed on $T[\rho]$, since it has been shown that the combination $\frac{1}{9}T_{WZ}[\rho] + T_{TF}[\rho]$ best approximates the kinetic energy in DFT.[56,71,73] Also, the electron-number-dependent terms (N) included in $s^3(\mathbf{r})$ and $s^4(\mathbf{r})$ correct for the excess kinetic energy contained in T_{WZ}. This correction is particularly relevant in the region where $\rho(\mathbf{r})$ is a function that varies slowly with the distance to the nucleus.

Using the well-established $s^1(\mathbf{r})$ as a reference, we have re-examined systems previously characterized through the NCI methodology of Contreras et al.,[51] including the water dimer, benzene dimer, methane dimer, and adenine-thymine nitrogen base pair, among others. To enhance the applicability of our RDG version, we performed NCI analysis on a DNA fragment using promolecular densities. More detailed information can be found in the supplementary information. Additionally, we discuss the performance of $s^n(\mathbf{r})$ concerning other RDG applications, such as calculating the charge associated with noncovalent interactions and chemical bonding analysis. This study was carried out using a modified version of the Multi-wavefunction Analyzer (Multiwfn),[77] which incorporates small Fortran subroutines specifically designed for this purpose. Information regarding the subroutines is available upon reasonable request from the authors.

Results and discussion

Despite the widespread use of NCI analysis based on $s(\mathbf{r})$, criticism regarding its fundamental nature has been relatively neglected in non-covalent interaction scenarios. Figure 1 illustrates the values of $s^n(\mathbf{r})$ for bicyclo[2.2.2]octane and both methane and water dimers. These molecules exhibit the three most common types of interactions—van der Waals interactions, hydrogen bonds, and repulsive interactions—typically identified through RDG analysis.

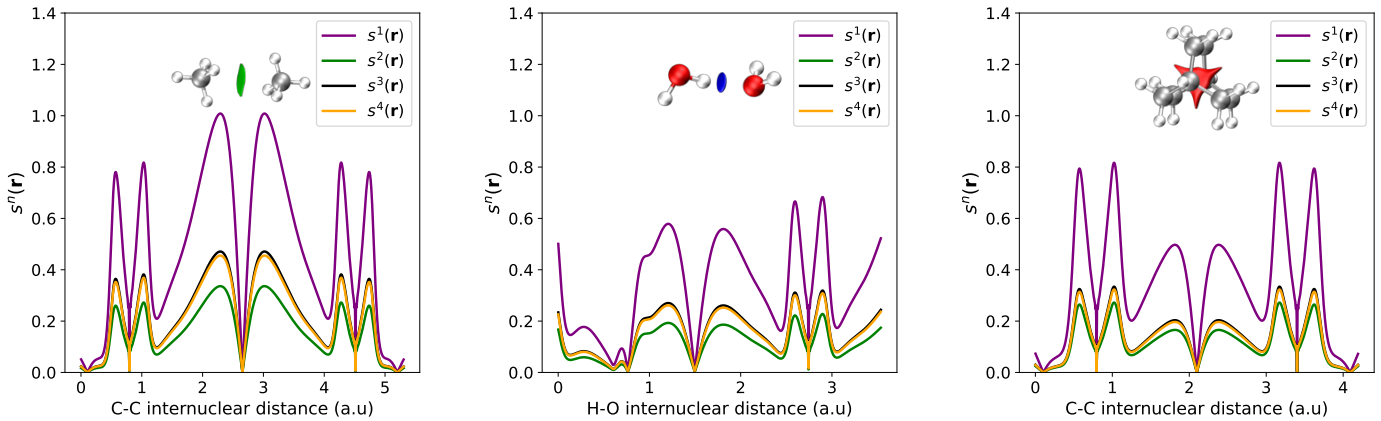

Figure 1: $s^n(\mathbf{r})$ for the methane dimer (Panel a), the water dimer (Panel b), and bicyclo[2.2.2]octane (Panel c), showing that low values of $s^n(\mathbf{r})$ correlate with regions where $\rho(\mathbf{r})$ varies slowly. It is worth mentioning that $s^1(\mathbf{r}) = s(\mathbf{r})$.

The description provided by $s^1(\mathbf{r})$ and $s^n(\mathbf{r})$ follows the same trend. Particularly, near the nuclear positions associated with C, O, and H atoms, as well as intermolecular regions where weak interactions typically occur. However, $s^2(\mathbf{r})$, $s^3(\mathbf{r})$, and $s^4(\mathbf{r})$ exhibit smaller values compared to $s^1(\mathbf{r})$ due to the correction on $\tau_{TF}(\mathbf{r})$ and $\tau_{WZ}(\mathbf{r})$, which are reflected by the local momentum behavior. This means that the critical points of $s^n(\mathbf{r})$ are associated with regions where $\nabla\rho(\mathbf{r}) \to 0$. Consequently, in regions of low $s^n(\mathbf{r})$ the $\rho(\mathbf{r})$ varies slowly, which is frequently assumed when interpreting RDG.

While $s^n(\mathbf{r}) \leq s^1(\mathbf{r})$, the optimal formulation of $s(\mathbf{r})$ for characterizing non-covalent interactions remains an open question. Exploring a potential solution involves delving into

the theoretical framework of DFT. It is essential to bear in mind that, despite $s(\mathbf{r})$ exhibiting a general dependence on $\rho(\mathbf{r})$, it is inseparable from the N-electron problem from which it originated. It is a well-established fact that the accuracy of GGA functionals relies heavily on the convergence of the gradient expansion, particularly as it diverges for terms of higher order $(n > 4)$.[55] This divergence leads to issues in estimating energy and, consequently, results in poorly-behaved electron densities. Thus, it is imperative to ensure that the regions bounded by the function $s(\mathbf{r})$ are adequately defined, ensuring a well-behaved electron density $\rho(\mathbf{r})$. It is worth emphasizing that the qualitative description of NCI analysis unequivocally depends on the curvature of $\rho(\mathbf{r})$. As such, precision and rigor in defining $\rho(\mathbf{r})$ are essential for a meaningful NCI analysis. It is necessary to explore the limit condition associated with the NCI model.

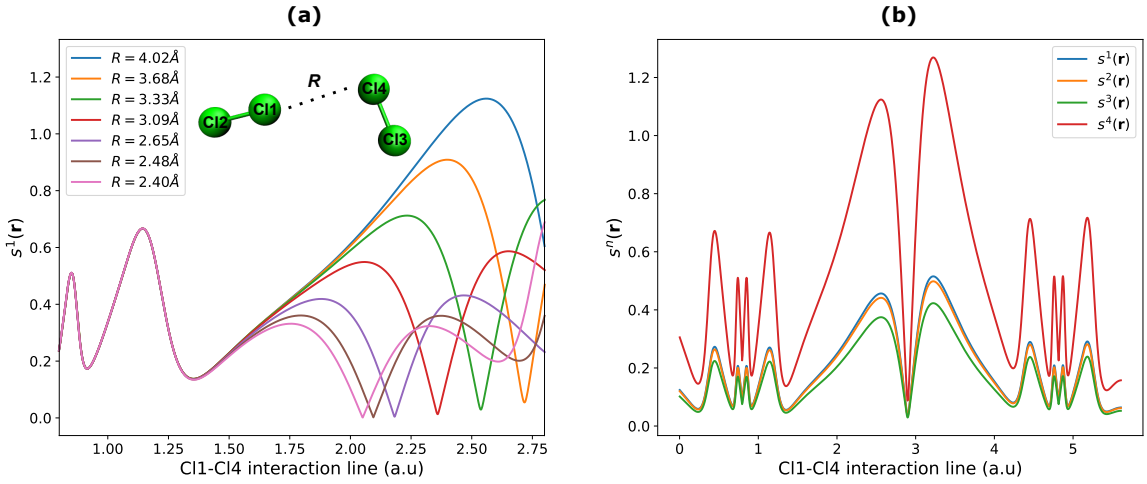

Figure 2: In Panel a, $s^1(\mathbf{r})$ tends to the unity for $Cl_1 \cdots Cl_4$ distances greater that 3.5 $\mathring{A}$. This indicates the regions where gradient expansions can lead to convergence issues. In Panel b, $s^4(\mathbf{r})$ displays the highest sensitivity, although all the functions show a similar trend for the Cl_2 dimer. It is worth noting that $s^1(\mathbf{r}) = s(\mathbf{r})$.

The $Cl_2 \cdots Cl_2$ dimer is a suitable system for exploring the $s(\mathbf{r}) \to \infty$ as $\rho(\mathbf{r}) \to 0$ relationship, as depicted in Figure 2. This suggests that in regions of low electron density, the disparities between $P_{WZ}(\mathbf{r})$ and $P_{TF}(\mathbf{r})$ would be negligible, thereby precluding the emergence of an asymptotic behavior of $s(\mathbf{r})$. Nevertheless, such a conclusion overlooks

the relevance of NCIs concerning long-range domains involving low electron densities. $s^1(\mathbf{r})$ augments as the Cl-Cl distance increases, tending to the unity for distances greater than 3.5 $\mathring{A}$. This result is particularly relevant since high values of $s^1(\mathbf{r})$ are associated with problems in gradient expansion in the DFT context, where this function behaves poorly.

The inequality:

$$\underbrace{\frac{\nabla\rho(\mathbf{r})}{2C_F\rho(\mathbf{r})^{4/3}}}_{s(\mathbf{r})} < 1 \tag{11}$$

gives the necessary condition for the convergence of the gradient expansion, which is essential for high-quality kinetic energy functionals.[60] Diverging values correspond to unreliable electron densities. Regardless of the method used to calculate $\rho(\mathbf{r})$, the function $s^1(\mathbf{r})$ continues to represent the inherent strengths or limitations of the model from which it is elucidated. In this context, the analysis of long-range interactions using the most popular version of RDG questions the physical source of $s(\mathbf{r})$'s high values as $\rho(\mathbf{r}) \to 0$.

Moreover, the fulfillment of the following condition is also relevant in regions where $\rho(\mathbf{r})$ exhibits slow variation:[60]

$$\underbrace{\frac{\nabla^2\rho(\mathbf{r})}{2C_F\rho(\mathbf{r})^{1/3}\nabla\rho(\mathbf{r})}}_{q(\mathbf{r})} \ll 1 \tag{12}$$

Domains delimited by $s(\mathbf{r})$ should be restricted and/or scrutinized using $q(\mathbf{r})$. $q(\mathbf{r})$ is critical in addressing inhomogeneities in the electron gas and defining the convergence of the KED gradient expansion. The Cl_2 dimer unveils a surprising correlation between $s^n(\mathbf{r})$ and $q(\mathbf{r})$, particularly $q(\mathbf{r})$ tends to 1 as $s^1(\mathbf{r})$ approaches this value; see Figure 3.

Conversely, the values of $q(\mathbf{r})$ are closer to 0.5 for $s^2(\mathbf{r})$, $s^3(\mathbf{r})$, and $s^4(\mathbf{r})$. This indicates the NCIs description provided by these new functions is more fine-tuned, as they delimit regions matching equation (12) better than the popular $s(\mathbf{r})$. Consequently, future NCI analysis must consider the $q(\mathbf{r})$ criterion. The versions of $s(\mathbf{r})$ proposed in this manuscript are better suited to satisfy inequalities (12) and (13), potentially signifying a conceptual

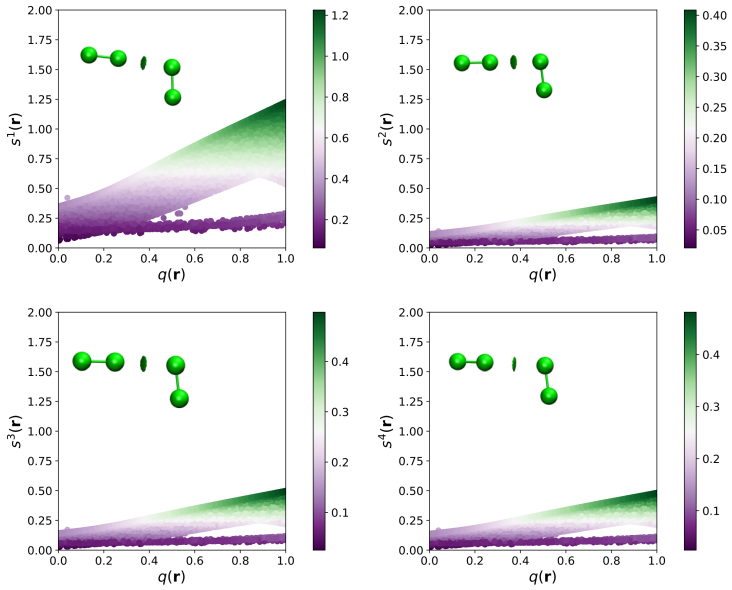

Figure 3: The proposed functions $s^2(\mathbf{r})$ (Panel b), $s^3(\mathbf{r})$ (Panel c), and $s^4(\mathbf{r})$ (Panel d) perform better than the popular $s(\mathbf{r})$ as they exhibit values < 0.50 for the Cl dimer. It is worth mentioning that $s^1(\mathbf{r}) = s(\mathbf{r})$.

advancement in the NCI analysis within the RDG framework.

Figure 4 presents a classical 2D NCI diagram for the Adenine-Thymine (AT) dimer, which allows assessing the performance of the proposed functions in distinguishing between repulsive and attractive interactions according to the sign of the second eigenvalue (λ_2) of the Hessian matrix of the electron density. A similar pattern is observed in the description provided by both the new, i.e., $s^2(\mathbf{r})$, $s^3(\mathbf{r})$, and $s^4(\mathbf{r})$ regarding the interactions in AT. As expected, steric effects associated with the 5- and 6-membered rings show repulsive character in regions bounded by $s^n(\mathbf{r})$. Peaks of $s^n(\mathbf{r})$ correspond to hydrogen bridges O $\cdots$ H formed between the carbonyl and amino groups, which appear in domains where $\lambda_2 < 0$. van der Waals' interactions between the adenine and thymine units are associated with values of $\lambda_2 \simeq 0$. Notably, the expression $s^1(\mathbf{r}) > s^n(\mathbf{r})$ holds for the A-T dimer. These results emphasize the robustness of modified versions of the RDG concerning NCI analysis.

As for the physical relevance of the regions defined by the RDG, methods other than partitioning the molecular space based on the gradient field of $s(\mathbf{r})$ have been explored so far. The zero-flux condition $s(\mathbf{r}) \cdot n(\mathbf{r}) = 0$ might allow bounding volumes associated with NCIs

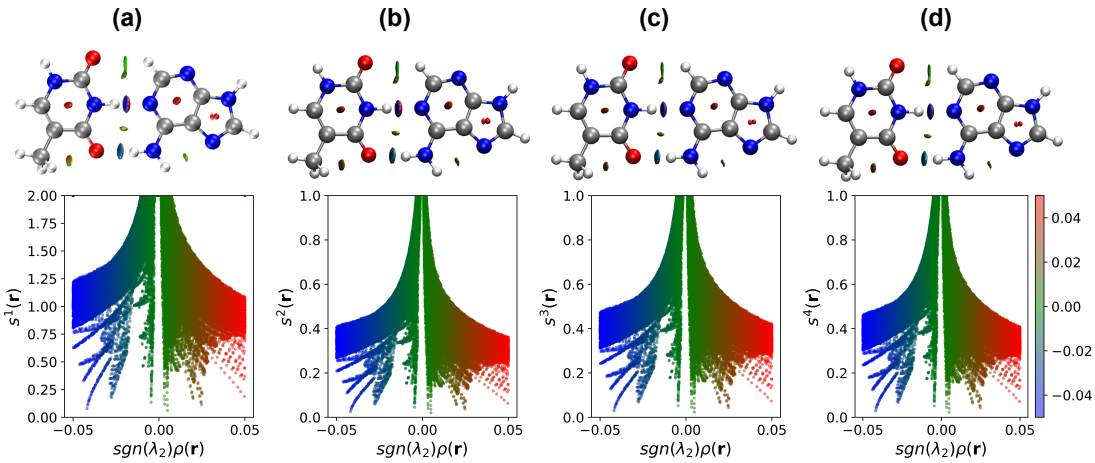

Figure 4: NCI diagrams for the adenine-thymine dimer. Notably, the new functions $s^2(\mathbf{r})$ (Panel b), $s^3(\mathbf{r})$ (Panel c), and $s^4(\mathbf{r})$ (Panel d) show lower values than $s(\mathbf{r})$. It is worth mentioning that $s^1(\mathbf{r}) = s(\mathbf{r})$.

(Ω_{NCI}).[78] Therefore, providing a definition of Ω_{NCI} that complies with the virial theorem[79] is a topic open to discussion. Although gauging this theorem to derive quantitative indices from properties such as volume is beyond the scope of NCI analysis, it plays a relevant role in defining Ω_{NCI}. The virial theorem has the local form:[2,79,80]

$$\int_{\Omega} 2G(\mathbf{r}) + V(\mathbf{r}) - \frac{1}{4}\nabla^2\rho(\mathbf{r}) = 0 \tag{13}$$

The symbols $G(\mathbf{r})$ and $V(\mathbf{r})$ denote the local kinetic energy density and the local potential energy density, respectively. Figure 5 illustrates Ω_{NCI} for different non-covalent interactions associated with $H_2S \cdots HCl$, $H_4C \cdots HF$, $C_2H_2 \cdots C_2H_4$, and $H_2O \cdots H_3N$. The numerical integration of equation (13) over these regions shows that Ω_{NCI} derived from the proposed $s^n(\mathbf{r})$ fulfill the virial theorem, as presented in Table 1.

Although these outcomes may be promising, they do not constitute rigorous proof of the local virial form fulfillment, meaning that further studies are needed. The asymptotic behavior of $s(\mathbf{r})$ as $\rho(\mathbf{r})$ approaches 0 does not necessarily reflect a physical situation inherent

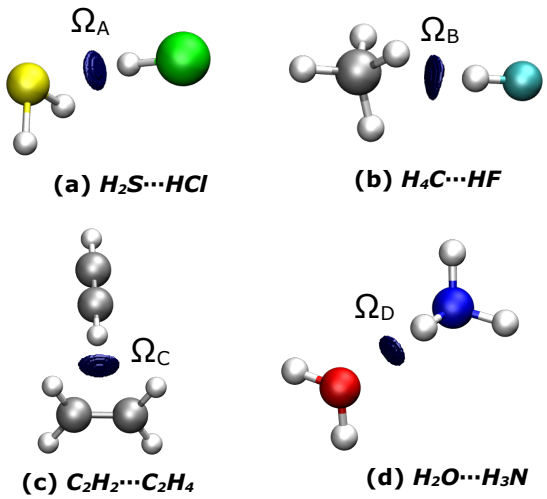

Figure 5: NCI volumes Ω_{NCI} obtained from the new $s^n(\mathbf{r})$ for the $H_2S \cdots HCl$ (Panel a), $H_4C \cdots HF$ (Panel b), $C_2H_2 \cdots C_2H_4$ (Panel c), and $H_2O \cdots H_3N$ (Panel d) systems.

Table 1: Values derived from integrating the local virial theorem (equation 13) over NCI volumes of the $H_2S \cdots HCl$ (Ω_A), $H_4C \cdots HF$ (Ω_B), $C_2H_2 \cdots C_2H_4$ (Ω_C), and $H_2O \cdots H_3N$ (Ω_D) systems. Units in Hartree.

	Ω_A	Ω_B	Ω_C	Ω_D
$s^1(\mathbf{r})$	-5.6×10^{-21}	-1.9×10^{-21}	-4.4×10^{-21}	1.1×10^{-19}
$s^2(\mathbf{r})$	5.2×10^{-21}	-1.1×10^{-19}	2.8×10^{-20}	-1.1×10^{-19}
$s^3(\mathbf{r})$	-1.9×10^{-21}	8.6×10^{-21}	-4.3×10^{-21}	2.3×10^{-19}
$s^4(\mathbf{r})$	-1.72×10^{-19}	9.4×10^{-21}	-6.7×10^{-21}	2.4×10^{-19}

to molecular interactions. Indeed, $s(\mathbf{r})$ should not tend to a finite value in the absence of such interactions. This evidences that $s(\mathbf{r})$ fails in fully incorporating NCI's physics. The disparity between $P_{WZ}(\mathbf{r})$ and $P_{TF}(\mathbf{r})$ as $\rho(\mathbf{r})$ approaches 0 is the origin of the asymptotic behavior of $s(\mathbf{r})$.

In modeling electronic structures using density functionals, the kinetic energy functional is defined in terms of Fermi and Weizacker KEDs. Thus, the following RDG form is proposed:

$$\mathrm{NRDG}(\mathbf{r}) = \frac{P_{WZ}(\mathbf{r})}{P_{WZ}(\mathbf{r}) + P_{TF}(\mathbf{r})} = \frac{|\nabla\rho(\mathbf{r})|}{|\nabla\rho(\mathbf{r})| + C_F\rho(\mathbf{r})^{4/3}} \tag{14}$$

In equation (14), the Fermi gas reference $P_{TF}(\mathbf{r})$ is replaced by the sum of local moments $P_{WZ}(\mathbf{r})$ and P_{TF} to incorporate a more realistic representation. This results in a dimen-

sionless NRDG($\mathbf{r}$), which is bounded between 0 and 1 and describes the inhomogeneity of the electron density at a specific point $\mathbf{r}$ within a molecular system. Unlike the unbounded RDG, NRDG allows evaluating the inhomogeneity portion of $\rho(\mathbf{r})$ within $P_{WZ}(\mathbf{r})$ rigorously. The NCI analysis using the NRDG($\mathbf{r}$) matches closely the derived from the classical version, as shown in Figure 6.

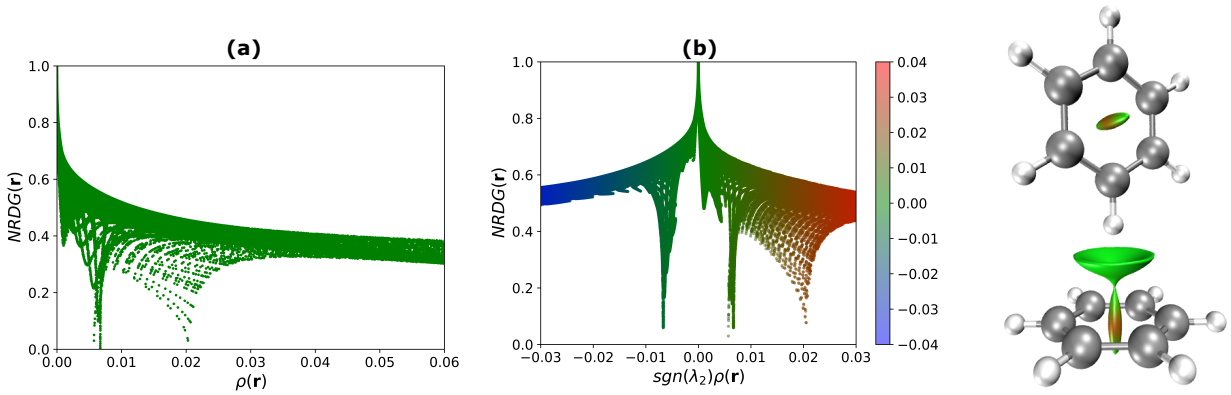

Figure 6: The proposed normalized RDG, NRDG, accurately describes the van der Waals and repulsive interactions for the benzene dimer indicated by the peaks at $\rho(\mathbf{r}) = 0.007$ and $\rho(\mathbf{r}) = 0.02$, respectively, (Panel a). The second eigenvalue of the Hessian matrix of the electron density further supports this result (Panel b).

The benzene dimer exhibits two types of interactions: i. the van der Waals interaction between the H atoms of one of the benzenes with the electronic cloud π of the remaining, which is evidenced by a peak at $\rho(\mathbf{r}) = 0.007$, ii. the repulsive, associated with the ring strains and signaled by the peak $\rho(\mathbf{r}) = 0.02$; see Figure 6, Panel a. These results can be derived from the curvature of NRDG($\mathbf{r}$) as well; see Figure 6, Panel b. The normalized RDG version allows incorporating suitable local functions $\tau_{WZ}(\mathbf{r})$ and $\tau_{TF}(\mathbf{r})$ to describe the slow and rapid variations of $\rho(\mathbf{r})$.

To this point, we have shown the need to formulate new versions of the RDG by deriving local moments from more rigorous KEDs, i.e., the models of Weizacker and Fermi. As a subsequent step, the $s^5(\mathbf{r})$ is derived from the local momentum representation, $P_G(\mathbf{r}) = \sqrt{\frac{2G(\mathbf{r})}{\rho(\mathbf{r})}}$), of the Lagrangian kinetic energy density $G(\mathbf{r})$, a more real-world KED.[61–63,81,82]

$$s^5(\mathbf{r}) = \frac{P_{WZ}(\mathbf{r})}{P_G(\mathbf{r})} = \frac{|\nabla\rho(\mathbf{r})|}{2\sqrt{2\rho(\mathbf{r})G(\mathbf{r})}} \tag{15}$$

It should be noted that the introduction of $G(\mathbf{r})$ in the RDG implies an explicit dependence on the orbitals rather than a dependence solely on $\rho(\mathbf{r})$. Figure 7 presents an NCI analysis based on $s^5(\mathbf{r})$ for the uracil dimer. The plot of $s^5(\mathbf{r})$ versus $\rho(\mathbf{r})$ shows characteristic peaks at low values of $s^5(\mathbf{r})$ (Figure 7, Panel a). Similar to the case of the popular $s^1(\mathbf{r})$, these interactions are classified as repulsive and attractive using $sgn(\lambda_2(\mathbf{r}))\rho(\mathbf{r})$ (Figure 7, Panels b and c).

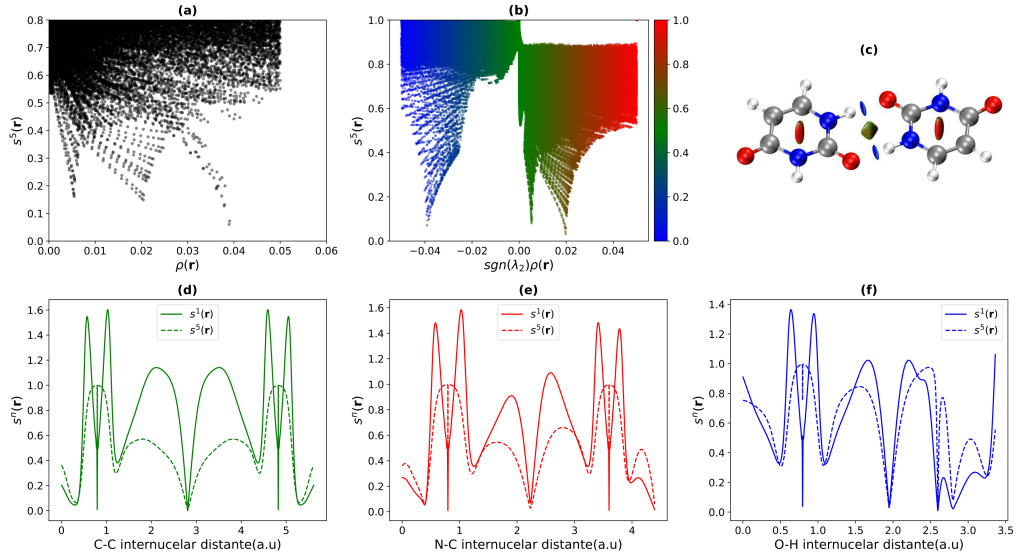

Figure 7: The Lagrangian kinetic-derived, $s^5(\mathbf{r})$, provides a reliable picture of NIC interactions for the uracil dimer, evidenced by the peaks at low $s^5(\mathbf{r})$ (Panels a-c). Remarkably, $s^5(\mathbf{r})$ exhibits lower values than $s^1(\mathbf{r})$ for the C-C (Panel d), N-C (Panel e), and O-H (Panel f) internuclear distances. It is worth emphasizing that $s^1(\mathbf{r}) = s(\mathbf{r})$.

$s^5(\mathbf{r})$ and $s^1(\mathbf{r})$ provide a similar description for C-C (van der Waals interaction), N-C (steric interaction) and N-H (hydrogen bonding). Particularly, in regions where $s^5(\mathbf{r}) = 0$. However, $s^5(\mathbf{r})$ exhibits smaller values. The latter feature is desirable, as high values of $s^1(\mathbf{r})$ could limit regions where $\rho(\mathbf{r})$ does not behave properly. The noticeable difference around the nuclei is expected as $P_{TF}(\mathbf{r})$ poorly describes the rapid changes in $rho(\mathbf{r})$; in contrast to the representation provided by $P_G(\mathbf{r})$, which considers the specificities of the system,

bypassing thus the Fermi gas model. It is important to stress that the implementation of the Lagrangian local momentum into the RDG equation requires additional computational cost, as it exhibits orbital dependence.

The purpose of this manuscript is to demonstrate that the RDG can be written in several ways to describe NCIs, without replacing its current version, but rather to have alternatives for its calculation. In addition, the existence of these versions also brings into discussion its physical foundations since the uniqueness of the RDG in the analysis of molecular interactions does not hold. Our RDG formulations offer mainly conceptual improvements for characterizing noncovalent interactions. Alternative expressions, including $s^2(\mathbf{r})$, $s^3(\mathbf{r})$, $s^4(\mathbf{r})$, and $s^5(\mathbf{r})$, provide a more rigorous definition of NCI volumes and address normalization issues encountered in the original RDG framework. These formulations feature enhanced delineation of interaction volumes and normalization procedures that overcome non-physical behaviors. By revising the expressions for Weizacker and Fermi kinetic energies based on DFT framework, our approach ensures better alignment with physical models since corrected versions of such quantities are included within RDG equation.

Conlusions

The effectiveness of the popular reduced electron density gradient (RDG) in qualitatively characterizing non-covalent interactions (NCIs) is well-documented. However, challenges persist in interpreting its results and understanding its physical significance, mainly because it is arbitrarily extracted from the GGA formalism, lacking a mathematical demonstration that establishes its connection to the underlying physics of NCIs. We have shown the feasibility of enhancing RDG to identify a local function directly relevant to NCIs by modifying the local kinetic energy densities (KEDs). Therefore, new versions capable of characterizing the nature of NCIs were derived. Notably, refining the local moments based on the Weizacker and Thomas-Fermi KEDs yielded four well-founded RDG versions, providing high-quality results comparable with the established formulation. From a theoretical viewpoint, these

surprising findings indicate the non-existence of a unique way to define the RDG scalar field to characterize NCIs. Exploring other virial local relationships within RDG-defined volumes and quantities in GGA approximations could provide key insights, thereby deepening our understanding of using RDG to characterize non-covalent interactions.

Supporting Information

Derivation of $s^n(\mathbf{r})$; Isosurfaces of $s^1(\mathbf{r})$, $s^2(\mathbf{r})$, $s^3(\mathbf{r})$ and $s^4(\mathbf{r})$ for several molecular systems and DNA fragments.

Acknowledgements

The authors thank the ANID/CONICYT PhD scholarship awarded to J. Burgos. Also, we are indebted to the Fondo Nacional de Ciencia y Tecnología (FONDECYT-ANID, Chile) for the continuous financial and academic support provided through Project No. 1231018 (EC).

References

(1) Bader, R. F. A quantum theory of molecular structure and its applications. *Chemical Reviews* **1991**, *91*, 893–928.

(2) Bader, R. F. Atoms in molecules. *Accounts of chemical research* **1985**, *18*, 9–15.

(3) Savin, A.; Nesper, R.; Wengert, S.; Fässler, T. F. ELF: The electron localization function. *Angewandte Chemie International Edition in English* **1997**, *36*, 1808–1832.

(4) Silvi, B.; Savin, A. Classification of chemical bonds based on topological analysis of electron localization functions. *Nature* **1994**, *371*, 683–686.

(5) Johnson, E. R.; Keinan, S.; Mori-Sánchez, P.; Contreras-García, J.; Cohen, A. J.; Yang, W. Revealing Noncovalent Interactions. *Journal of the American Chemical Society* **2010**, *132*, 6498–6506.

(6) Fradera, X.; Austen, M. A.; Bader, R. F. The Lewis model and beyond. *The Journal of Physical Chemistry A* **1999**, *103*, 304–314.

(7) Pendás, Á. M.; Francisco, E.; Suárez, D.; Costales, A.; Díaz, N.; Munárriz, J.; Rocha-Rinza, T.; Guevara-Vela, J. M. Atoms in molecules in real space: a fertile field for chemical bonding. *Physical Chemistry Chemical Physics* **2023**, *25*, 10231–10262.

(8) Bader, R. F.; MacDougall, P. J. Toward a theory of chemical reactivity based on the charge density. *Journal of the American Chemical Society* **1985**, *107*, 6788–6795.

(9) Chermette, H. Chemical reactivity indexes in density functional theory. *Journal of computational chemistry* **1999**, *20*, 129–154.

(10) Racioppi, S.; Sironi, A.; Macchi, P. On generalized partition methods for interaction energies. *Physical Chemistry Chemical Physics* **2020**, *22*, 24291–24298.

(11) Khojandi, M.; Zahedi, E.; Seif, A.; Taghvamanesh, A.; Karimkhani, M. A Theoretical Study on the Degenerate Cope Rearrangement of Hypostrophene Using the RRKM Theory and Topological Approaches. *ChemistrySelect* **2021**, *6*, 1607–1615.

(12) Taherian, R.; Chahkandi, B.; Zahedi, E. A comprehensive theoretical analysis of Curtius rearrangement of syn-syn and syn-anti conformers of oxalyl diazide. *Journal of Molecular Graphics and Modelling* **2021**, *109*, 108012.

(13) Ayarde-Henríquez, L.; Guerra, C.; Duque-Noreña, M.; Chamorro, E. Unraveling the role of the electron-pair density symmetry in reaction mechanism patterns: the Newman–Kwart rearrangement. *New Journal of Chemistry* **2022**, *46*, 12002–12009.

(14) Kula, K.; Kacka-Zych, A.; Łapczuk-Krygier, A.; Jasiński, R. Analysis of the possibility and molecular mechanism of carbon dioxide consumption in the Diels-Alder processes. *Pure and Applied Chemistry* **2021**, *93*, 427–446.

(15) Kacka-Zych, A.; Pérez, P. Perfluorobicyclo [2.2. 0] hex-1 (4)-ene as unique partner for Diels–Alder reactions with benzene: a density functional theory study. *Theoretical Chemistry Accounts* **2021**, *140*, 1–16.

(16) Kacka-Zych, A. Understanding the uniqueness of the stepwise [4+ 1] cycloaddition reaction between conjugated nitroalkenes and electrophilic carbene systems with a molecular electron density theory perspective. *International Journal of Quantum Chemistry* **2021**, *121*, e26440.

(17) Ayarde-Henríquez, L.; Guerra, C.; Duque-Noreña, M.; Rincón, E.; Pérez, P.; Chamorro, E. Are There Only Fold Catastrophes in the Diels–Alder Reaction Between Ethylene and 1, 3-Butadiene? *The Journal of Physical Chemistry A* **2021**, *125*, 5152–5165.

(18) Ayarde-Henríquez, L.; Guerra, C.; Duque-Noreña, M.; Rincón, E.; Pérez, P.; Chamorro, E. On the Notation of Catastrophes in the Framework of Bonding Evolution Theory: Case of Normal and Inverse Electron Demand Diels-Alder Reactions. *ChemPhysChem* **2022**, *23*, e202200343.

(19) Chamorro, E.; Guerra, C.; Ayarde-Henríquez, L.; Duque-Noreña, M.; Pérez, P.; Rincón, E. New insights from a bonding evolution theory based on the topological analysis of the electron localization function. *Chemical Reactivity* **2023**, 465–481.

(20) Guerra, C.; Ayarde-Henríquez, L.; Duque-Norena, M.; Chamorro, E. On electron pair rearrangements in photochemical reactions: 1, 3-cyclohexadiene ring opening. *The Journal of Physical Chemistry A* **2021**, *126*, 395–405.

(21) Guerra, C.; Ayarde-Henriquez, L.; Duque-Noreña, M.; Cárdenas, C.; Pérez, P.; Chamorro, E. On the nature of bonding in the photochemical addition of two ethylenes: C–C bond formation in the excited state? *Physical Chemistry Chemical Physics* **2021**, *23*, 20598–20606.

(22) Guerra, C.; Ayarde-Henríquez, L.; Duque-Noreña, M.; Chamorro, E. Unraveling the Bonding Nature Along the Photochemically Activated Paterno-Büchi Reaction Mechanism. *ChemPhysChem* **2021**, *22*, 2342–2351.

(23) Guerra, C.; Ayarde-Henríquez, L.; Duque-Noreña, M.; Chamorro, E. Photochemically induced 1, 3-butadiene ring-closure from the topological analysis of the electron localization function viewpoint. *ChemPhysChem* **2022**, *23*, e202200217.

(24) Guerra, C.; Ayarde-Henríquez, L.; Rodríguez-Núñez, Y. A.; Ensuncho, A.; Chamorro, E. Elucidating the N- N and C- N Bond-breaking Mechanism in the Photoinduced Formation of Nitrile Imine. *ChemPhysChem* **2023**, *24*, e202200867.

(25) Guerra, C.; Ayarde-Henríquez, L.; Chamorro, E.; Ensuncho, A. Uncovering Triradicaloid Structures in S1 Benzene Photochemistry. *ChemPhotoChem* **2023**, *7*, e202200263.

(26) Guerra, C.; Ayarde-Henríquez, L.; Rodriguez-Nuñez, Y. A.; Chamorro, E.; Ensuncho, A. E. Mechanistic insights into benzyne formation via 1, 2-di-iodobenzene photolysis. *New Journal of Chemistry* **2023**, *47*, 21270–21275.

(27) Krokidis, X.; Noury, S.; Silvi, B. Characterization of elementary chemical processes by catastrophe theory. *The Journal of Physical Chemistry A* **1997**, *101*, 7277–7282.

(28) Ayarde-Henríquez, L.; Guerra, C.; Duque-Noreña, M.; Chamorro, E. Revisiting the bonding evolution theory: a fresh perspective on the ammonia pyramidal inversion and bond dissociations in ethane and borazane. *Physical Chemistry Chemical Physics* **2023**, *25*, 27394–27408.

(29) Ayarde-Henríquez, L.; Guerra, C.; Chamorro, E. From Local Topology to Molecular Geometries via Minimizing the Total Energy: The Pyrolysis of Cubane. *ChemRxiv, http://doi.org/10.26434/chemrxiv-2023-kjrbc.*

(30) Seif, A.; Domingo, L. R.; Zahedi, E.; Ahmadi, T. S.; Mazarei, E. Unraveling the kinetics and molecular mechanism of gas phase pyrolysis of cubane to [8] annulene. *RSC advances* **2020**, *10*, 32730–32739.

(31) Ayarde-Henríquez, L.; Lupi, J.; Dooley, S. Hemicellulose pyrolysis: mechanism and kinetics of functionalized xylopyranose. *Physical Chemistry Chemical Physics* **2024**, *26*, 12820–12837.

(32) Ayarde-Henríquez, L.; Guerra, C.; Duque-Noreña, M.; Chamorro, E. A simple topology-based model for predicting the activation barriers of reactive processes at 0 K. *Physical Chemistry Chemical Physics* **2023**, *25*, 14274–14284.

(33) Zhong, S.; He, X.; Liu, S.; Wang, B.; Lu, T.; Rong, C.; Liu, S. Toward Density-Based and Simultaneous Description of Chemical Bonding and Noncovalent Interactions with Pauli Energy. *The Journal of Physical Chemistry A* **2022**, *126*, 2437–2444, PMID: 35389639.

(34) Rong, C.; Zhao, D.; He, X.; Liu, S. Development and Applications of the Density-Based Theory of Chemical Reactivity. *The Journal of Physical Chemistry Letters* **2022**, *13*, 11191–11200, PMID: 36445239.

(35) Liu, S.; Rong, C.; Lu, T.; Hu, H. Identifying Strong Covalent Interactions with Pauli Energy. *The Journal of Physical Chemistry A* **2018**, *122*, 3087–3095, PMID: 29489374.

(36) Mackenzie, C. F.; Spackman, P. R.; Jayatilaka, D.; Spackman, M. A. CrystalExplorer model energies and energy frameworks: extension to metal coordination compounds, organic salts, solvates and open-shell systems. *IUCrJ* **2017**, *4*, 575–587.

(37) Saleh, G.; Gatti, C.; Presti, L. L. Non-covalent interaction via the reduced density gradient: Independent atom model vs experimental multipolar electron densities. *Computational and Theoretical Chemistry* **2012**, *998*, 148–163.

(38) Kleemiss, F.; Dolomanov, O. V.; Bodensteiner, M.; Peyerimhoff, N.; Midgley, L.; Bourhis, L. J.; Genoni, A.; Malaspina, L. A.; Jayatilaka, D.; Spencer, J. L.; et al. Accurate crystal structures and chemical properties from NoSpherA2. *Chemical Science* **2021**, *12*, 1675–1692.

(39) Tariq, A.; Nazir, S.; Arshad, A. W.; Nawaz, F.; Ayub, K.; Iqbal, J. DFT study of the therapeutic potential of phosphorene as a new drug-delivery system to treat cancer. *RSC advances* **2019**, *9*, 24325–24332.

(40) Sagaama, A.; Issaoui, N.; Al-Dossary, O.; Kazachenko, A. S.; Wojcik, M. J. Non covalent interactions and molecular docking studies on morphine compound. *Journal of King Saud University-Science* **2021**, *33*, 101606.

(41) Yang, S.-Y.; Qu, Y.-K.; Liao, L.-S.; Jiang, Z.-Q.; Lee, S.-T. Research Progress of Intramolecular π-Stacked Small Molecules for Device Applications. *Advanced Materials* **2022**, *34*, 2104125.

(42) Kasai, H.; Tolborg, K.; Sist, M.; Zhang, J.; Hathwar, V. R.; Filsø, M. Ø.; Cenedese, S.; Sugimoto, K.; Overgaard, J.; Nishibori, E.; et al. X-ray electron density investigation of chemical bonding in van der Waals materials. *Nature materials* **2018**, *17*, 249–252.

(43) Yar, M.; Hashmi, M. A.; Ayub, K. Nitrogenated holey graphene (C2N) surface as highly selective electrochemical sensor for ammonia. *Journal of Molecular Liquids* **2019**, *296*, 111929.

(44) Jena, S.; Dutta, J.; Tulsiyan, K. D.; Sahu, A. K.; Choudhury, S. S.; Biswal, H. S. Noncovalent interactions in proteins and nucleic acids: Beyond hydrogen bonding and π-stacking. *Chemical Society Reviews* **2022**, *51*, 4261–4286.

(45) Manjunatha, B.; Bodke, Y. D.; Nagaraja, O.; Nagaraju, G.; Sridhar, M. Coumarin-benzothiazole based azo dyes: synthesis, characterization, computational, photophysical and biological studies. *Journal of Molecular Structure* **2021**, *1246*, 131170.

(46) Barroso, J.; Cabellos, J. L.; Pan, S.; Murillo, F.; Zarate, X.; Fernandez-Herrera, M. A.; Merino, G. Revisiting the racemization mechanism of helicenes. *Chemical Communications* **2018**, *54*, 188–191.

(47) Armstrong, A.; Boto, R. A.; Dingwall, P.; Contreras-Garcia, J.; Harvey, M. J.; Mason, N. J.; Rzepa, H. S. The Houk–List transition states for organocatalytic mechanisms revisited. *Chemical Science* **2014**, *5*, 2057–2071.

(48) Emamian, S.; Lu, T.; Kruse, H.; Emamian, H. Exploring nature and predicting strength of hydrogen bonds: A correlation analysis between atoms-in-molecules descriptors, binding energies, and energy components of symmetry-adapted perturbation theory. *Journal of computational chemistry* **2019**, *40*, 2868–2881.

(49) Kozuch, S.; Martin, J. M. Halogen bonds: Benchmarks and theoretical analysis. *Journal of chemical theory and computation* **2013**, *9*, 1918–1931.

(50) Laplaza, R.; Peccati, F.; A. Boto, R.; Quan, C.; Carbone, A.; Piquemal, J.-P.; Maday, Y.; Contreras-García, J. NCIPLOT and the analysis of noncovalent interactions using the reduced density gradient. *WIREs Computational Molecular Science* **2021**, *11*, e1497.

(51) Contreras-García, J.; Boto, R. A.; Izquierdo-Ruiz, F.; Reva, I.; Woller, T.; Alonso, M. A benchmark for the non-covalent interaction (NCI) index or... is it really all in the geometry? *Theoretical Chemistry Accounts* **2016**, *135*, 1–14.

(52) Boto, R. A.; Contreras-García, J.; Tierny, J.; Piquemal, J.-P. Interpretation of the reduced density gradient. *Molecular Physics* **2016**, *114*, 1406–1414.

(53) Boto, R. A.; Piquemal, J.-P.; Contreras-García, J. Revealing strong interactions with the reduced density gradient: a benchmark for covalent, ionic and charge-shift bonds. *Theoretical Chemistry Accounts* **2017**, *136*, 1–9.

(54) Ziesche, P.; Kurth, S.; Perdew, J. P. Density functionals from LDA to GGA. *Computational materials science* **1998**, *11*, 122–127.

(55) Perdew, J. P.; Burke, K.; Ernzerhof, M. Generalized gradient approximation made simple. *Physical review letters* **1996**, *77*, 3865.

(56) García-Aldea, D.; Alvarellos, J. Kinetic energy density study of some representative semilocal kinetic energy functionals. *The Journal of chemical physics* **2007**, *127*, 144109.

(57) Della Sala, F.; Fabiano, E.; Constantin, L. A. Kinetic-energy-density dependent semilocal exchange-correlation functionals. *International Journal of Quantum Chemistry* **2016**, *116*, 1641–1694.

(58) Clark, T. How deeply should we analyze non-covalent interactions? *Journal of Molecular Modeling* **2023**, *29*, 66.

(59) Lu, T.; Chen, Q. Interaction Region Indicator: A Simple Real Space Function Clearly Revealing Both Chemical Bonds and Weak Interactions**. *Chemistry–Methods* **2021**, *1*, 231–239.

(60) Sahni, V.; Gruenebaum, J.; Perdew, J. Study of the density-gradient expansion for the exchange energy. *Physical Review B* **1982**, *26*, 4371.

(61) Yang, Z.; Wang, A. Y.; Liu, S.-B. On the single-electron local kinetic energy. *Science in China Series B: Chemistry* **1998**, *41*, 174–181.

(62) Jiang, H. The local kinetic energy density revisited. *New Journal of Physics* **2020**, *22*, 103050.

(63) Anderson, J. S.; Ayers, P. W.; Hernandez, J. I. R. How ambiguous is the local kinetic energy? *The Journal of Physical Chemistry A* **2010**, *114*, 8884–8895.

(64) Ernzerhof, M. The role of the kinetic energy density in approximations to the exchange energy. *Journal of Molecular Structure: THEOCHEM* **2000**, *501*, 59–64.

(65) Hamilton, I.; Mosna, R. A.; Site, L. D. Classical kinetic energy, quantum fluctuation terms and kinetic-energy functionals. *Theoretical Chemistry Accounts* **2007**, *118*, 407–415.

(66) Ludeña, E. V. On the nature of the correction to the Weizsacker term. *The Journal of Chemical Physics* **1982**, *76*, 3157–3160.

(67) Acharya, P. K.; Bartolotti, L. J.; Sears, S. B.; Parr, R. G. An atomic kinetic energy functional with full Weizsacker correction. *Proceedings of the National Academy of Sciences* **1980**, *77*, 6978–6982.

(68) Garcia-Aldea, D.; Alvarellos, J. E. Generalized nonlocal kinetic energy density functionals based on the von Weizsäcker functional. *Physical Chemistry Chemical Physics* **2012**, *14*, 1756–1767.

(69) Gázquez, J.; Robles, J. On the atomic kinetic energy functionals with full Weizsacker correction. *The Journal of Chemical Physics* **1982**, *76*, 1467–1472.

(70) Deb, B.; Chattaraj, P. New quadratic nondifferential Thomas-Fermi-Dirac-type equation for atoms. *Physical Review A* **1988**, *37*, 4030.

(71) Tomishima, Y.; Yonei, K. Solution of the Thomas-Fermi-Dirac equation with a modified Weizsäcker correction. *Journal of the Physical Society of Japan* **1966**, *21*, 142–153.

(72) Englert, B.-G. Energy functionals and the Thomas-Fermi model in momentum space. *Physical Review A* **1992**, *45*, 127.

(73) Salasnich, L. Kirzhnits gradient expansion for a D-dimensional Fermi gas. *Journal of Physics A: Mathematical and Theoretical* **2007**, *40*, 9987.

(74) Cohen, L. Local values in quantum mechanics. *Physics Letters A* **1996**, *212*, 315–319.

(75) Bohórquez, H. J.; Boyd, R. J. On the local representation of the electronic momentum operator in atomic systems. *The Journal of chemical physics* **2008**, *129*, 024110.

(76) Bohórquez, H. J.; Boyd, R. J. A localized electrons detector for atomic and molecular systems. *Theoretical Chemistry Accounts* **2010**, *127*, 393–400.

(77) Lu, T.; Chen, F. Multiwfn: A multifunctional wavefunction analyzer. *Journal of computational chemistry* **2012**, *33*, 580–592.

(78) Bader, R. F. The zero-flux surface and the topological and quantum definitions of an atom in a molecule. *Theoretical chemistry accounts* **2001**, *105*, 276–283.

(79) Bader, R. F.; Beddall, P. Virial field relationship for molecular charge distributions and the spatial partitioning of molecular properties. *The Journal of Chemical Physics* **1972**, *56*, 3320–3329.

(80) Cremer, D.; Kraka, E. A description of the chemical bond in terms of local properties of electron density and energy. *Croatica Chemica Acta* **1984**, *57*, 1259–1281.

(81) Espinosa, E.; Alkorta, I.; Rozas, I.; Elguero, J.; Molins, E. About the evaluation of the local kinetic, potential and total energy densities in closed-shell interactions. *Chemical physics letters* **2001**, *336*, 457–461.

(82) Bader, R. F.; Essén, H. The characterization of atomic interactions. *The Journal of chemical physics* **1984**, *80*, 1943–1960.

TOC Graphic